Available online at www.sciencedirect.com
SCIENCE DIRECT
Journal of Catalysis 239 (2006) 42–50
JOURNAL OF CATALYSIS
www.elsevier.com/locate/jcat

Hydroamination of 1,3-cyclohexadiene with aryl amines catalyzed with acidic form zeolites

Oriol Jimenez [a], Thomas E. Müller [a,*], Wilhelm Schwieger [b], Johannes A. Lercher [a]

[a] *Lehrstuhl II für Technische Chemie, Technische Universität München, Lichtenbergstraße 4, D-85747 Garching, Germany*
[b] *Lehrstuhl für Chemische Reaktionstechnik, Friedrich-Alexander-Universität Erlangen-Nürnberg, Egerlandstr. 3, D-91058 Erlangen, Germany*

Received 17 October 2005; revised 23 December 2005; accepted 6 January 2006

Available online 9 February 2006

Abstract

The intermolecular hydroamination of 1,3-cyclohexadiene with aniline using zeolite catalysts was investigated. The reaction mechanism and the influence of amine basicity on the rate of reaction were studied. Zeolite H-BEA was the most active catalyst, whereas the incorporation of Zn^{2+} (Zn/H-BEA) led to decreasing catalytic activity, indicating that the reaction is catalyzed by Brønsted acid sites. Subtle shape selective effects determine the reactivity and selectivity of the zeolites.

Keywords: Hydroamination; 1,3-Cyclohexadiene; Aniline; Substituent effects; Catalysis; Ion exchange; Zeolite; Characterization

1. Introduction

Catalytic hydroamination is a chemical route with high synthetic potential allowing the formation of a variety of nitrogen-containing molecules by the direct addition of amines to alkenes and alkynes [1–3]. Compared with other methods for the synthesis of amines, enamines, and imines [4], hydroamination offers one of the most attractive pathways to such molecules. Conceptionally, the desired higher-substituted nitrogen-containing products are formed in a single reaction step from inexpensive alkenes and alkynes without the intrinsic formation of side products [5,6]. Various transition metals are known to be suitable as molecular catalysts for both inter and intramolecular hydroamination of alkenes and alkynes [7]; for example, titanium, ruthenium, palladium, and copper complexes have been used as catalysts for intramolecular and intermolecular hydroamination of alkynes, allenes, and activated alkenes [8–14].

Intermolecular hydroamination of dienes is more difficult than hydroamination of alkynes, and only few catalysts are known. Nucleophilic addition of amines to 1,3-dienes with sodium and alkyllithium salts provides primarily 1,4-addition products. Other regioisomers are formed as byproducts [4]. Lanthanum complexes can efficiently catalyze the intramolecular hydroamination of aminodienes to nitrogen-containing heterocycles [15]. Yoshifuji et al. [16] reported the use of palladium complexes to obtain a high product yield for the addition of anilines to 1,3-dienes. A recent study reported on the use of a liquid–liquid two-phase system to catalyze the intermolecular hydroamination of terminal alkynes and dienes with anilines [17]. The use of acids as co-catalysts can enhance the catalytic activity of palladium in the addition of aniline to dienes [18]. A similar influence of Brønsted acids was also observed for the reaction of vinylarenes with arylamines [19]. The role of acid is still under investigation [20]; in most cases, the addition of acid seems to prevent oligomerisation of the dienes, as well as telomerisation of two or more olefin molecules with one amine molecule [19,21].

Although a number of homogeneous catalysts for hydroamination reactions are well known, only a few examples of heterogeneous catalysts have been reported. The amination of isobutene with ammonia to *tert*-butylamine occurs over Re-Y-zeolite with >90% selectivity [22]; however, this catalyst suffers from rapid deactivation. BASF has developed an iron silicate zeolite catalyst of the pentasil type that not only shows >99% selectivity, but also affords a commercially acceptable catalyst life [23,24]. Ion-exchanged zeolites [25,26] and immo-

* Corresponding author.
E-mail address: Thomas.Muller@ch.tum.de (T.E. Müller).

0021-9517/$ – see front matter
doi:10.1016/j.jcat.2006.01.007

bilized zinc salts [27] have been used successfully for the cyclisation of 6-aminohex-1-yne, and immobilized transition metal complexes have been used in the addition of 4-isopropylaniline to phenylacetylene [28].

The present work addresses the use of Beta, ZSM-5, Faujasite, and Mordenite as catalysts for the intermolecular hydroamination of 1,3-cyclohexadiene with aryl amines. Zeolite H-BEA in particular has been shown to be a good solid acid catalyst, especially for reactions involving bulky transition states, such as isobutene/*n*-butene alkylation [29,30], and is in the focus of this study. Special attention is given to the influence of amine basicity on the rate of reaction.

2. Experimental

2.1. General

All reagents were obtained from Aldrich and were used as received. Zinc-exchanged zeolites were prepared by repeated ion exchange of the corresponding H-BEA zeolite (Südchemie AG, T-4546, MA039 Hr99) in an aqueous solution of $Zn(CH_3CO_2)_2$ as described previously [26]. The material was dried and calcined, and the metal loading was determined by atomic absorption spectroscopy (AAS). The Zn/H-BEA zeolites had a loading in the range of 0.03–0.54 $mmol_{Zn^{2+}}\ g^{-1}$ catalyst. The H-MFI (H-MFI 220, EX 717 H1-C) and H-MOR (H-MOR 90, SN 302 H/01) zeolites were supplied by Südchemie. H-FAU zeolite (CBV 400) was obtained from Zeolyst International. H-BEA zeolites with different crystal sizes were prepared at Friedrich-Alexander-Universität Erlangen-Nürnberg.

Catalytic experiments were performed under inert nitrogen atmosphere in a Radleys reaction carousel with 12 parallel reactors. The zeolite (0.25 g) was activated overnight at 200 °C in vacuum. It was suspended in toluene (15 cm^3), and the mixture was heated to reflux at 111 °C. Aniline (91 μL, 1 mmol) and 1,3-cyclohexadiene (196 μL, 2 mmol) were added. Samples (50 μL) for gas chromatography (GC) analyses were obtained at regular intervals. GC analyses were performed on a Hewlett–Packard HP 5890A gas chromatograph equipped with a cross-linked 5% diphenyl–95% dimethyl–polysiloxane column (30 m, Restek GmbH, Rtx-5 Amine). GC–mass spectroscopy (GC-MS) analyses were performed on a Hewlett–Packard HP 5890 gas chromatograph equipped with an identical column and a mass selective detector (HP 5971A). Peak areas were referenced to *n*-dodecane as an internal standard. Reactions at temperatures above the boiling point of toluene were performed in a 300-cm^3 Parr autoclave. The apparent activation energy was determined in the temperature range 110–200 °C, and the reaction order in aniline was determined in the concentration range 20–140 $mmol\,L^{-1}$. To study the influence of the aniline basicity, aniline was replaced with substituted anilines.

2.2. Physical and analytical methods

The Si/Al ratio was determined by AAS using a UNICAM 939 spectrometer. Surface area, pore diameter, and pore size distribution of the catalysts were determined by nitrogen adsorption (Sorptomatic 1990 Series instrument) after activation of the samples at 250 °C in vacuum.

Temperature-programmed desorption (TPD) profiles were measured in a custom-built 6-port parallel setup. The catalysts were pelletized, and a 20-mg sample was placed into each quartz tube. The samples were activated at 450 °C in vacuum (at 1×10^{-3} mbar) for 1 h, then cooled to 150 °C, and ammonia was adsorbed at 3 mbar for 10 min. After saturation, the samples were outgassed for 1 h to remove physisorbed ammonia. Subsequently, the temperature was increased at a rate of $10\,°C\,min^{-1}$, with the desorption process monitored by MS (Balzers QMS 200).

For infrared (IR) spectroscopic measurements, a self-supporting sample wafer was placed into a sorption cell and activated at 450 °C in vacuum for 1 h. The sample was cooled to 150 °C, and pyridine was adsorbed at 10^{-1} mbar for 1 h. After saturation, the sample was outgassed at 150 °C for 1 h. IR spectra of the activated sample were recorded in the region of 4000–400 cm^{-1} at a resolution of 4 cm^{-1} using a Perkin–Elmer 2000 spectrometer. The sample was then heated to 450 °C at a rate of $10\,°C\,min^{-1}$, then outgassed for 1 h. The temperature was subsequently reduced to 150 °C, and another IR spectrum was obtained. The concentration of acid sites was estimated from the intensity of the bands at 1544 and 1455 cm^{-1}, assigned to pyridinium ions (Brønsted acid sites, $\varepsilon = 1.67\ cm\,\mu mol^{-1}$) and coordinatively bound pyridine (Lewis acid sites, $\varepsilon = 2.22\ cm\,\mu mol^{-1}$), respectively, using molar extinction coefficients reported previously [31].

Scanning electron microscopy images were obtained on a JEOL 500 SEM microscope. Samples were outgassed for 1 day and sputtered with gold. Images were taken by operating the microscope at 23.0 kV.

3. Results and discussion

3.1. Catalyst characterization

Three samples of zeolite H-BEA with different particle sizes but similar Si/Al ratios (11.6–14.9), as well as H-ZSM-5, H-Mordenite, and H-Y, and a series of zinc-exchanged Zn/H-BEA zeolites (zinc content 0.03–0.54 $mmol\,g^{-1}$), were used in this study. To facilitate understanding of the performance of the zeolites in catalysis, the H-BEA, H-ZSM-5, H-Mordenite, and H-Y samples were fully characterized beforehand (Table 1). A detailed characterization of the Zn/H-BEA zeolites was recently published [32].

Particle sizes were determined from scanning electron microscopy images. The three H-BEA samples (abbreviated as BEA1, BEA2, and BEA3) consisted of crystallites with particle sizes of 0.15–0.20, 0.20–0.25, and 0.60–0.70 μm, respectively (Fig. 1). However, closer inspection showed that each particle was an agglomerate composed of much smaller primary particles (approximately 50–70 nm in diameter). Micropore volume slightly decreased with particle size (0.135, 0.129, and 0.112 $ml\,g^{-1}$, respectively), indicating that fewer pores can be accessed as the crystallites become larger. H-ZSM-5,

Table 1
Physicochemical properties of the H-Zeolites used in this study

Catalyst	Structure	Ratio Si/Al	Pore diameter[a] (Å)	Particle size (μm)	Surface area[b] ($m^2\,g^{-1}$)	MSA[c] ($m^2\,g^{-1}$)	Micropore volume ($ml\,g^{-1}$)	BAS[d] ($mmol_{Py}\,g^{-1}$)	LAS[e] ($mmol_{Py}\,g^{-1}$)	TPD ($mmol_{NH_3}\,g^{-1}$)
H-ZSM-5	MFI	45	5.1 × 5.5 [100] 5.3 × 5.6 [010]	0.40–0.50	359	191	0.084	0.21	0.09	0.35
H-Mordenite	MOR	45	6.5 × 7.0 [001] 2.6 × 5.7 [001]	0.50–0.60	418	284	0.138	0.14	0.02	0.33
H-Y	FAU	2.7	7.4 × 7.4 [111]	0.40–0.50	527	415	0.209	0.22	0.31	0.77
H-BEA1	BEA	14.2	6.6 × 6.7 [100] 5.6 × 5.6 [001]	0.15–0.20	541	391	0.135	0.17	0.14	0.63
H-BEA2	BEA	11.6	6.6 × 6.7 [100] 5.6 × 5.6 [001]	0.20–0.25	624	359	0.129	0.19	0.14	0.41
H-BEA3	BEA	14.9	6.6 × 6.7 [100] 5.6 × 5.6 [001]	0.60–0.70	679	348	0.112	0.16	0.14	0.30

[a] The crystallographic direction is given in square brackets.
[b] BET surface area determined by N_2 adsorption.
[c] Micropore surface area (MSA) determined by N_2 adsorption.
[d] Brønsted acid site (BAS) concentration determined by pyridine (Py) adsorption.
[e] Lewis acid site (LAS) concentration determined by pyridine adsorption.

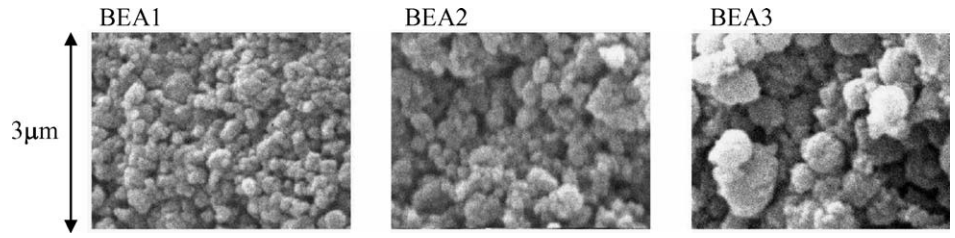

Fig. 1. SEM Micrographs of the H-BEA zeolites used in this study.

H-Mordenite, and H-Y had particle sizes in similar ranges (0.40–0.50, 0.50–0.60, and 0.40–0.50 μm, respectively).

The acidity of the zeolite samples was assessed by TPD of ammonia and from infrared spectra after adsorption of pyridine. The TPD traces of ammonia desorbing from the three H-BEA zeolites are presented in Fig. 2. The traces show two desorption maxima at ca. 340 and 560 °C. The low-temperature peak is characteristic for desorption of ammonia from weak acid sites, whereas the high-temperature peak is related to desorption of ammonia from strong acid sites. Deconvolution of the two peaks using a linear combination of Gauss functions [33] has shown that 0.48, 0.28, and 0.22 $mmol\,g^{-1}$ of ammonia desorbs from the weak acid sites and 0.15, 0.13, and 0.08 $mmol\,g^{-1}$ of ammonia desorbs from the strong acid sites for the BEA1, BEA2, and BEA3 samples, respectively. From the entire amount of ammonia adsorbed on BEA1, the overall acid site density was calculated to 0.63 $mmol\,g^{-1}$. With increasing particle size, this value decreased to 0.41 $mmol\,g^{-1}$ for BEA2 and to 0.30 $mmol\,g^{-1}$ for BEA3. This strongly suggests that the pore system is less accessible for ammonia molecules at larger particle sizes. However, because ammonia sorbs unspecifically [34] on Brønsted acid sites (BAS) and Lewis acid sites (LAS), assignment of the low- and high-temperature peaks is somewhat ambiguous. The overall acid site densities for H-ZSM-5, H-Mordenite, and H-Y were in the same range (0.35, 0.33, and 0.77 $mmol\,g^{-1}$, respectively).

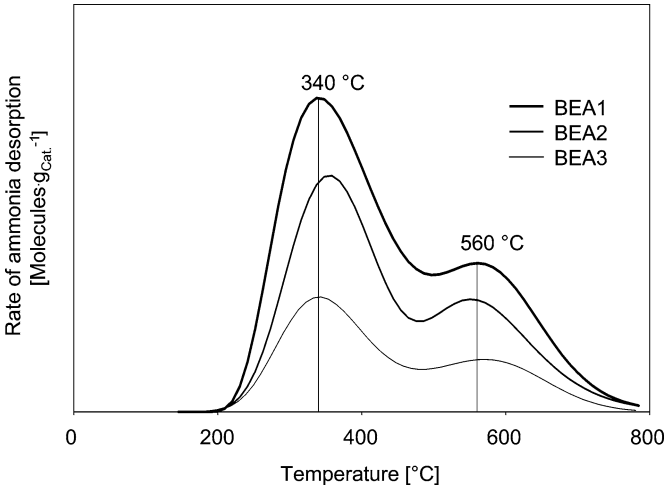

Fig. 2. TPD profiles for desorption of ammonia from H-BEA zeolites.

The IR spectra of activated zeolites exhibited several bands for isolated and bridging OH groups (Fig. 3). The most intense bands, attributed to external SiOH groups, were observed at 3739 cm^{-1} for BEA1 and at 3742 cm^{-1} for BEA2 and BEA3. The inherent high concentration of defect sites in BEA leads to a high concentration of internal silanol groups, which then become clearly visible in the IR spectrum. These OH groups frequently form hydrogen bonds, which give rise to the band

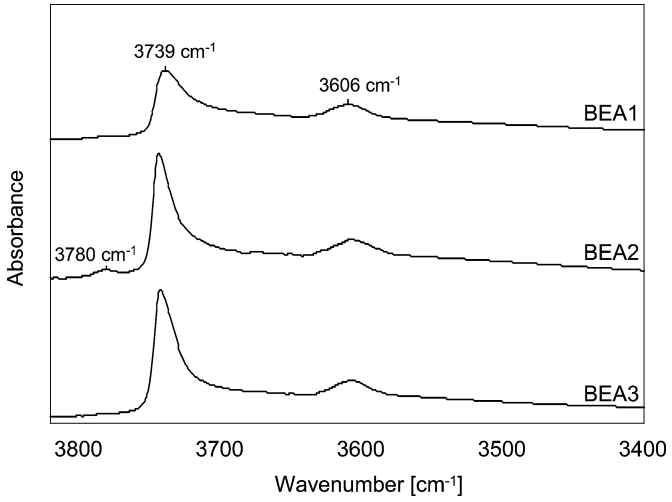

Fig. 3. Infrared spectra of the hydroxyl region of the H-BEA zeolites.

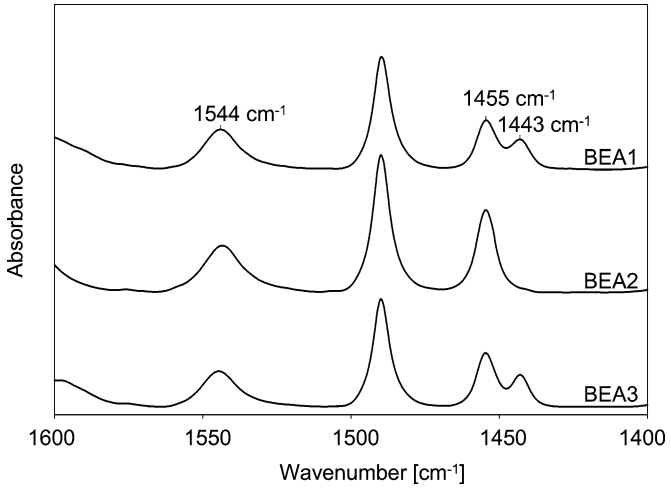

Fig. 4. Infrared spectra of the H-BEA zeolites after pyridine adsorption.

tailing from 3700 cm^{-1} down to 3300 cm^{-1} [35]. The band at 3606 cm^{-1}, observed at nearly the same intensity in all samples (0.062, 0.078, and 0.067 normalized absorbance units for BEA1, BEA2, and BEA3, respectively), corresponds to bridging hydroxyl groups, which give rise to strong Brønsted acidity of the material [36]. For BEA2, the additional band with low intensity observed at 3780 cm^{-1} is assigned to AlOH groups of extra-framework alumina.

After pyridine adsorption at 150 °C, the two bands at 3606 and 3780 cm^{-1} vanished completely. This shows that these OH groups are fully accessible to pyridine. In contrast, the peaks in the silanol region remained nearly unchanged after pyridine adsorption. This confirms the weak acidity of the external silanol OH protons [37]. The broad adsorption band at 3700–3400 cm^{-1} also appears to be sensitive to pyridine adsorption, albeit to a much lesser extent.

The ring vibrations of adsorbed pyridine were used to quantify the acid site concentration (Fig. 4). The BAS were identified by the peak at 1544 cm^{-1} (pyridinium ions). Only minor differences in the BAS concentration were observed for the three samples (0.16–0.19 mmol g^{-1}; see Table 1). Note that the BAS concentration was independent of the zeolite particle size. After desorption of pyridine by heating to 450 °C for 1 h, the concentration of pyridinium ions decreased dramatically. In BEA1, all pyridine was removed by this procedure, whereas for BEA2 and BEA3, the BAS concentration decreased to 0.04 and 0.03 mmol g^{-1}, respectively. Thus, BEA2 and BEA3 contained higher proportions of strong BAS than BEA1.

The LAS generally associated with accessible Al^{3+} cations gave rise to a peak at 1455 cm^{-1} (coordinatively bound pyridine). In the spectra of pyridine adsorbed on BEA1 and BEA3, a further peak at 1443 cm^{-1} was observed. This peak is probably related to sodium cations remaining from the preparation process [38]. Quantitative analysis showed that BEA1 and BEA3 contained 0.68 and 0.66 wt% sodium, respectively, whereas the sodium concentration in H-BEA2 was 0.01 wt%. From the combined intensity of the peaks at 1443 and 1455 cm^{-1}, the same LAS concentration (0.14 mmol g^{-1}) was measured for all three samples. After outgassing at 450 °C, the concentration of pyridine adsorbed on the LAS of BEA2 was reduced by approximately 16%, to 0.12 mmol g^{-1}, whereas for BEA1 and BEA3, the concentration of adsorbed pyridine molecules decreased by 50%, to 0.07 and 0.08 mmol g^{-1}, respectively. Pyridine molecules, which gave rise to the band at 1443 cm^{-1}, were completely removed by outgassing at 450 °C. This observation is consistent with assignment to weakly acidic sodium cations.

3.2. Catalytic measurements

The addition of aniline to 1,3-cyclohexadiene was studied as model reaction for hydroamination. The three samples of H-BEA with different particles sizes, a series of Zn/H-BEA zeolites with varying zinc contents, and various H-zeolites with different pore diameters were used as catalysts. All zeolites except H-ZSM-5 catalyzed the reaction, providing cyclohex-2-enyl-phenylamine (**1**) as the main product. More detailed analysis of the product mixture indicated the formation of structural isomers with differing double-bond positions (Fig. 5).

At short reaction times, the formal 1,4 and 1,2 addition products **1** and cyclohex-3-enyl-phenylamine (**2**) were formed in parallel. Note that the 2,1 addition product is indistinguishable from the 1,4 addition product. At longer reaction times, isomer **1** became the main product, and the concentration of isomer **2** decreased (Fig. 6). In parallel, the concentration of cyclohex-1-enyl-phenylamine (**3**) increased. In contrast, the formation of the Schiff-base cyclohexylidene-phenylamine (**4**) was not observed. This can be rationalized by a much lower thermodynamic stability of isomer **4**, probably caused by steric conflict between the β-protons of the phenyl and cyclohexylidene ring, which prevents parallel alignment of the phenyl ring and the C=N π-system. At very long reaction times, increasing amounts of di-(cyclohex-2-enyl)-phenylamine (**5**) were observed, resulting from the addition of two 1,3-cyclohexadiene molecules to one aniline molecule.

The reaction profile can be well described based on the model shown in Fig. 7, which enables one to derive the rate constants of the individual reaction steps. For the model, irre-

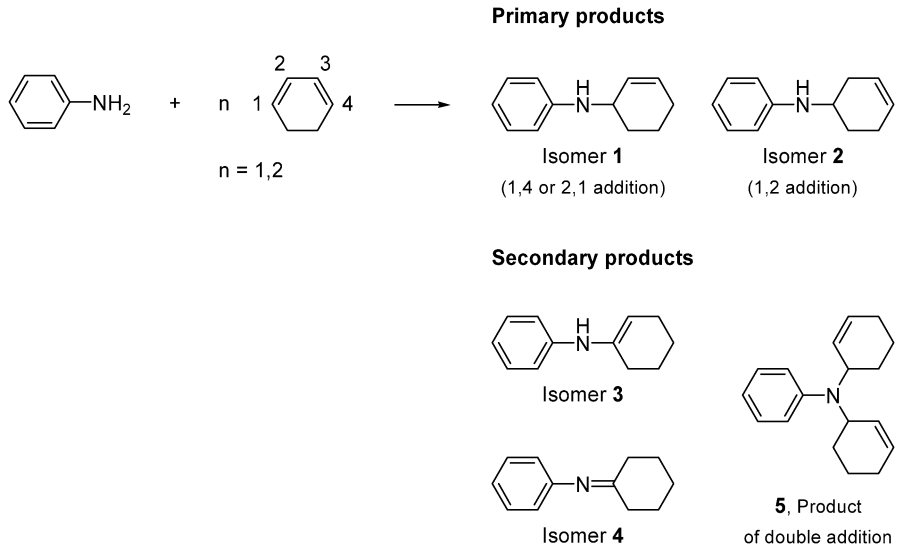

Fig. 5. Possible reaction products from the addition of aniline to 1,3-cyclohexadiene.

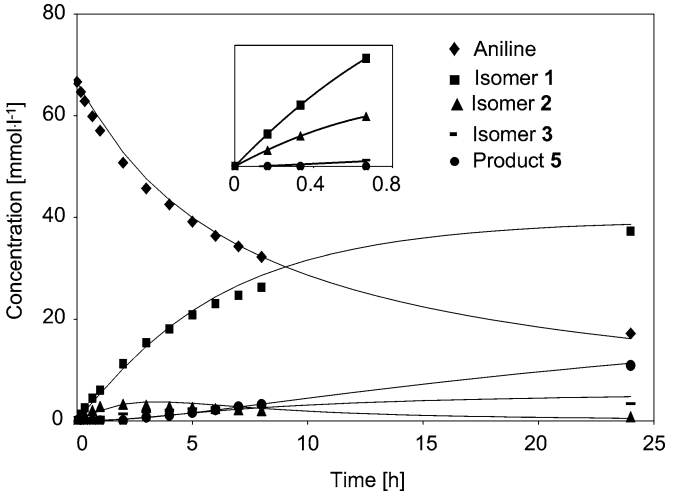

Fig. 6. Reaction profile of the reaction between 1,3-cyclohexadiene and aniline using H-BEA as catalyst. The continuous lines describe the concentration profile derived from the kinetic model given in Fig. 7.

versibility of the reactions and first order in all reactants were assumed. In this respect, the reaction order for aniline was determined to 0.93 in the concentration range 20–140 mmol L^{-1}.

Note that the fitted lines (Fig. 6) appear to slightly underestimate the overall reactivity with respect to the disappearance of the reactant and the appearance of product **1**, whereas there is a minor overestimation of their concentration at the end of the reaction. This suggests that the catalysts deactivate slightly with reaction time. An accurate estimation of the deactivation was beyond the scope of this study, however.

For BEA2, isomer **1** ($k_1 = 0.94$ (mmol $L^{-1})^{-1}$ h^{-1}) was formed three times faster than isomer **2** ($k_2 = 0.33$ (mmol $L^{-1})^{-1}$ h^{-1}). Product **2** isomerised to **1** ($k_{2-1} = 2.84$ h^{-1}) almost 10 times faster than it was formed. Isomer **1** isomerised to **3** or reacted to the double-addition product **5** with rate constants of $k_{1-3} = 0.16$ h^{-1} and $k_{1-5} = 2.84$ (mmol $L^{-1})^{-1}$ h^{-1}, respectively. All zeolites except ZSM-5 followed the same reaction sequence, in which the rate constant was higher for the reaction **2** → **1** than for the formation of isomer **2**.

The influence of potentially catalytically active Lewis acidic cations, such as Zn^{2+}, on the rate of intermolecular hydroamination was explored for a series of ion-exchanged zeolites Zn/H-BEA2 with zinc concentrations of 0.03–0.54 mmol g^{-1}. The catalysts were initially selected because they showed excellent catalytic properties for the intramolecular cyclisation of 6-

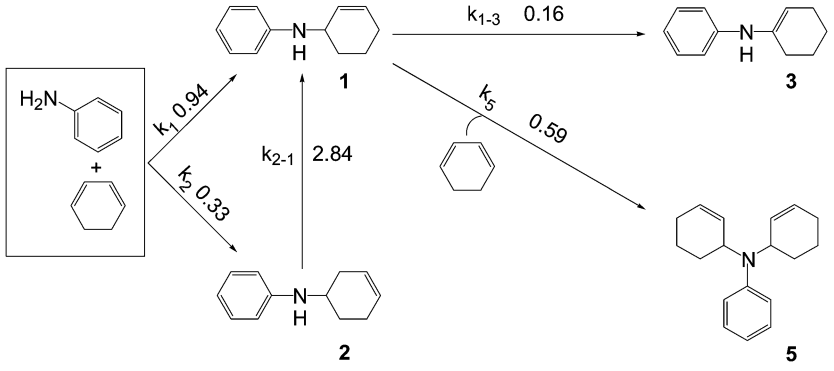

Fig. 7. Kinetic model for the hydroamination of 1,3-cyclohexadiene with aniline using H-BEA2 as catalyst; units: k_1, k_2, k_5 in (mmol $L^{-1})^{-1}$ h^{-1}; k_{2-1}, k_{1-3} in h^{-1}.

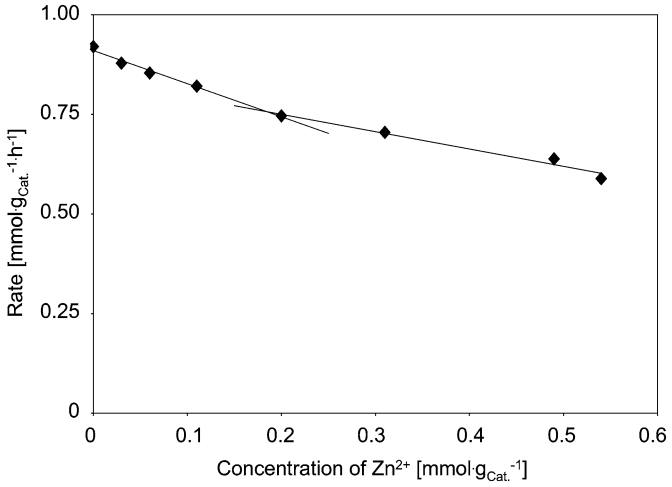

Fig. 8. Initial rate of formation of isomer **1** with a series of Zn/H-BEA catalyst varying in zinc contents.

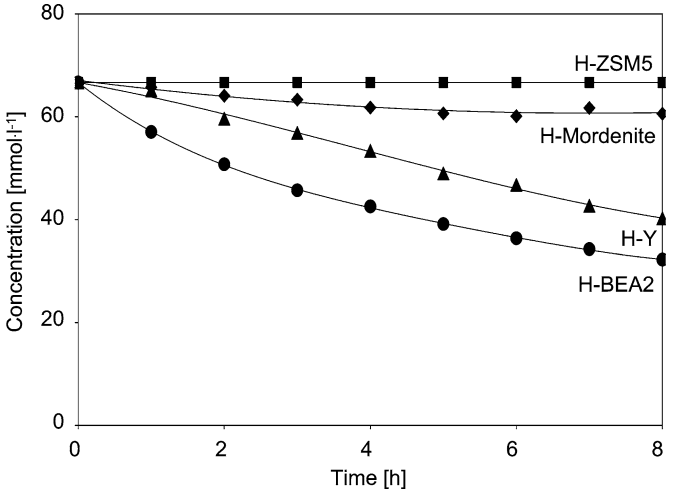

Fig. 9. Aniline conversion for the reaction between 1,3-cyclohexadiene and aniline catalyzed by different H-zeolites.

amino-1-hexyne [25,39]. The experiments were performed using the same substrate:catalyst ratio (in weight). Consequently, the total amount of zinc in the reaction mixture was varied.

In contrast to our expectations, the initial catalytic activity decreased with zinc loading. The initial rate of hydroamination was 0.92 mmol $g_{Cat}^{-1}\,h^{-1}$ for the parent material and decreased to 0.59 mmol $g_{Cat}^{-1}\,h^{-1}$ for Zn/H-BEA2 with a zinc concentration of 0.54 mmol g^{-1}. This suggests that the zinc cations incorporated in BEA2 were catalytically not active or less active for this reaction. Two regions of Zn^{2+} loading can be distinguished with a linear decrease in the activity of the material (Fig. 8). For the same series of zeolites, two regions of catalytic activity were equally observed for the addition of aniline to phenylacetylene and the cyclisation of 6-aminohex-1-yne, although the rate increased with zinc loading [26].

At low zinc concentrations, the zinc cations are exchanged for protons, reducing the concentration of those BAS, which exist so close to each other that the zinc cations can coordinate to both sites [32]. Note the steeper decline of the catalytic activity with increasing zinc concentration for these materials. At higher zinc concentrations ($\geqslant$0.20 mmol g^{-1}), the zinc is present in the zeolite pores mainly as nanosized ZnO clusters, which influence the Brønsted acidity of the zeolite to a lesser degree [32].

The total concentration of LAS increased from 0.14 mmol g^{-1} for the parent H-BEA zeolite (BEA2) to 0.20 mmol g^{-1} for the catalyst with the highest zinc loading [32]. In contrast, the BAS concentration decreased with the zinc exchange degree from 0.19 to 0.16 mmol g^{-1}. The catalytic activity closely followed the trend in the concentration of BAS. Thus, the BAS seem to be responsible for the catalytic activity, whereas the Zn^{2+} cations in the zeolite are inactive for the reaction. It should be noted, however, that a molecular Brønsted acid (trifluoromethanesulfonic acid) did not catalyze the reaction. These observations indicate that a reaction intermediate is stabilized in the zeolite pores. In addition, LAS resulting from the presence of aluminium in the material may play a role in the catalytic cycle.

To explore the potential role of the zeolite structure for the addition of aniline to 1,3-cyclohexadiene, fully ammonia-exchanged and -activated Brønsted acidic zeolites (without metal cations at exchange positions) with different pore diameters were examined. In particular, the catalytic activity of H-ZSM-5, H-Mordenite, and H-Y was compared with that of H-BEA zeolite. For all zeolites, the rate of reaction was reduced (Fig. 9). No reaction was observed for H-ZSM-5.

The reactants are able to access the acid sites of all zeolites used. Note, however, that the products face strong constraints to diffuse out of the pores. This is especially pronounced for H-ZSM-5, which has the smallest channel diameter. The larger, but one-dimensional, pores of Mordenite led to low activity with k_1 and k_2 values of 0.05 and 0.06 $(\text{mmol}\,L^{-1})^{-1}\,h^{-1}$, respectively (Table 2), whereas **5**, the product of double addition of 1,3-cyclohexadiene to aniline, was not observed. H-Y zeolite with a three-dimensional large pore system had nearly a sixfold-higher reaction rate (k_1 0.33 $(\text{mmol}\,L^{-1})^{-1}\,h^{-1}$ and k_2 0.33 $(\text{mmol}\,L^{-1})^{-1}\,h^{-1}$) than H-Mordenite; however, the supercage of H-Y is sufficiently large to allow formation of the double-addition product **5** [k_5 1.11 $(\text{mmol}\,L^{-1})^{-1}\,h^{-1}$; 38% yield after 24 h]. Zeolite BEA, on the other hand, has two interconnecting channel systems forming a smaller space than the faujasite supercage. Consequently, the reactants and the desired products can diffuse into and out of the pores, and the reaction rate is higher (k_1 and k_2 0.33 $(\text{mmol}\,L^{-1})^{-1}\,h^{-1}$). The product of the double addition is formed in lower amounts [k_5 0.59 $(\text{mmol}\,L^{-1})^{-1}\,h^{-1}$; 17% yield after 24 h]. The results suggest that the hydroamination reaction can be catalyzed most efficiently in the pores of a zeolite with 12-membered ring openings, such H-BEA zeolite, and that subtle shape selective effects determine reactivity and selectivity.

The influence of particle size was studied for the series of H-BEA zeolites with increasing particle sizes and similar BAS concentrations. The rates of reaction decreased with particle size (Fig. 10). Because the diameter of the micropores strongly influences the activity, we exclude the possibility that the reaction occurs exclusively at the pore entrance. The product for-

Table 2
Rate constants for single reactions steps and initial reaction rate for the hydroamination of 1,3-cyclohexadiene with aniline calculated on basis of the kinetic model given in Fig. 7

Catalyst	Hydroamination			Isomerisation		Initial rate[a]
	k_1 $((\text{mmol L}^{-1})^{-1}\,\text{h}^{-1})$	k_2 $((\text{mmol L}^{-1})^{-1}\,\text{h}^{-1})$	k_5 $((\text{mmol L}^{-1})^{-1}\,\text{h}^{-1})$	k_{2-1} (h^{-1})	k_{1-3} (h^{-1})	r_{ini} $(\text{mmol g}_{\text{Cat}}^{-1}\,\text{h}^{-1})$
H-ZSM-5	0.00	0.00	0.00	0.00	0.00	0.00
H-Mordenite	0.05	0.06	0.00	7.06	0.04	0.20
H-Y	0.33	0.33	1.11	6.18	0.09	0.58
H-BEA1	2.15	1.08	1.02	3.54	0.13	1.63
H-BEA2	0.94	0.33	0.59	2.84	0.16	0.92
H-BEA3	0.19	0.07	0.00	3.61	0.18	0.20

[a] Initial rate of aniline consumption.

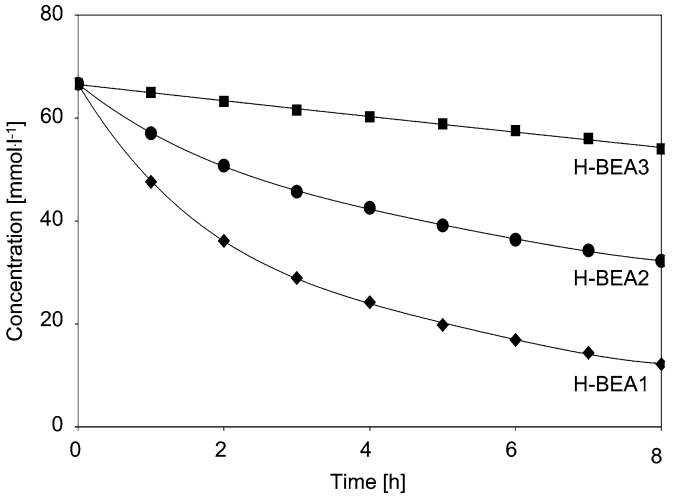

Fig. 10. Aniline conversion for the reaction between 1,3-cyclohexadiene and aniline catalyzed by H-BEA zeolites with different particle size.

mation constants for the BEA zeolites used in this study are reported in Table 2. The rate constants k_1 and k_2 clearly decreased with particle size. This is attributed to lower diffusive limitations in BEA1, whereas significant diffusion constrains appear likely for BEA2 and BEA3. Product **5**, which has a much larger kinetic diameter, is probably formed exclusively at the outer surface. The rate constant k_5 also decreased with particle size, confirming our conclusions on diffusion limitations. Formation of product **5** was not observed for BEA3. In contrast, isomerisation constants k_{2-1} and k_{1-3} are apparently unaffected by particle size.

For BEA2, low apparent activation energies of 45 kJ mol^{-1} based on aniline and 38 kJ mol^{-1} based on the main product of the reaction were determined in the temperature range 110–200 °C. These relatively low activation energies are consistent with pore diffusion limitations.

3.3. Proposed mechanism

The data obtained from the kinetic experiments suggest the mechanism shown in Fig. 11 for the intermolecular hydroamination of 1,3-cyclohexadiene with anilines using zeolite H-BEA as catalyst. The simplest kinetic model would start with a competitive adsorption between aniline and 1,3-cyclohexadiene on the BAS. Aniline, being a stronger base than 1,3-cyclohexadiene, is preferentially adsorbed. However, it is in equilibrium with the free BAS and can be displaced by the excess of 1,3-cyclohexadiene in the reaction mixture.

According to Yang et al. [40] alkenyl carbenium ions can be formed by direct protonation of dienes on acidic catalysts. The carbenium ions are strongly stabilised in zeolite by interaction with the BAS and more closely resemble an alkoxy group. For 1,3-cyclohexadiene [41], coordination to one of the BAS provides either a cation with delocalized charge (**a**) or the less-stable cation **b** [42]. Subsequent nucleophilic attack of the aniline on **a** or **b** leads to the intermediates $\mathbf{a}_1$ and $\mathbf{b}_1$, respectively. Subsequently, one of the ammonium protons is transferred to the BAS, and the products **1** and **2** are desorbed. Two possibilities exist for the nucleophilic attack during reaction pathway **a**, providing the formal 1,4 and 2,1 addition products. These two products are indistinguishable. Only reaction pathway **b** accounts for formation of the 1,2 addition product. After desorption, the primary reaction products **1** and **2** diffuse into the bulk solution and are readsorbed before isomerisation. This is also thought to occur on the BAS. An alternative reaction sequence with hydroamination and isomerisation in succession (without desorption and readsorption of the intermediates) can be excluded based on the kinetic model.

3.4. Influence of amine basicity

Because the reaction is acid-catalyzed, the basicity of the reacting amine could drastically change the reactant–catalyst interaction. Therefore, the influence of aniline basicity on the hydroamination of 1,3-cyclohexadiene was studied. Anilines with various substituents on the aromatic ring were used, particularly those with substituents in a *para* position to the NH_2 group. This allows us to change the basicity of the aniline without changing the minimum kinetic diameter of the molecule. Thus, it can be assumed that the *para*-substituted anilines have similar diffusion rates inside the zeolite pores.

The reaction rate decreased linearly with the basicity (lower pK_b) of the substituted aniline (Table 3; Fig. 12). 2-Methoxyaniline and parent aniline deviated from the correlation to lower and higher rates, respectively.

According to the proposed mechanism, aniline and 1,3-cyclohexadiene compete for coordination to the BAS. Because the substituted anilines are much more basic than 1,3-cyclohexadiene, formation of the anilinium ions is preferred. How-

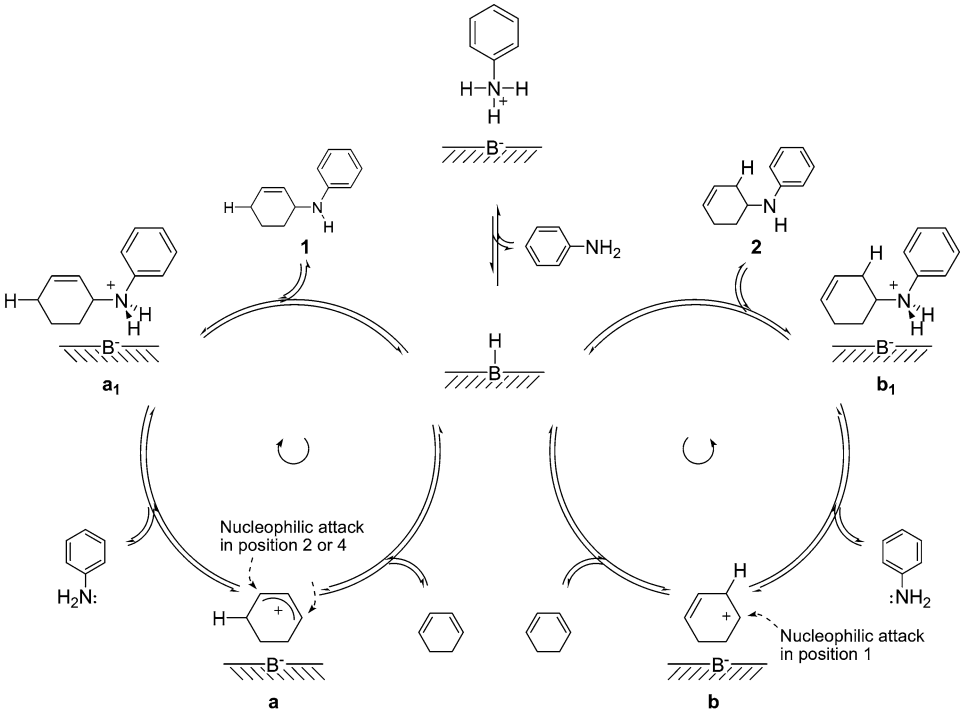

B–H, Brønsted acid site

Fig. 11. Proposed reaction mechanism for the intermolecular hydroamination of 1,3-cyclohexadiene with aniline catalyzed by H-BEA zeolites.

Table 3
Basicity (pK_b) of the arylamines used and rate of reaction in the hydroamination of 1,3-cyclohexadiene

Aromatic amine	Substituent	pK_b	Initial rate[a] (mmol g_{Cat}^{-1} h^{-1})	Isomer ratio[b] (%)
4-Methoxyaniline	*para* –OMe	8.7	0.19	90/5/5
4-Ethylaniline	*para* –Et	8.9	0.29	94/6/0
4-Fluoroaniline	*para* –F	9.3	0.48	97/3/0
Aniline	*para* –H	9.4	0.92	90/3/7
2-Methoxyaniline	*ortho* –OMe	9.5	0.17	93/0/7
3-Methoxyaniline	*meta* –OMe	9.8	0.79	94/3/3
4-Chloroaniline	*para* –Cl	10.0	0.82	94/0/6
Ethyl-4-aminobenzoate	*para* –COOEt	10.5	1.15	100/0/0
4-(Trifluoromethyl)aniline	*para* $-CF_3$	11.2	1.07	90/0/10
4-Nitroaniline	*para* $-NO_2$	13.0	1.80	100/0/0

[a] Initial rate of aniline consumption.
[b] After 24 h reaction time; ratio of isomers **1**, **2**, and **3**, respectively.

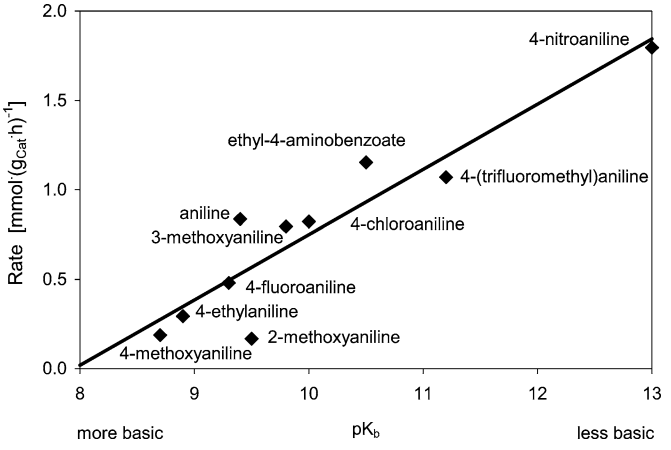

Fig. 12. Correlation between the initial rate of the addition of aniline to 1,3-cyclohexadiene and the basicity of the aniline.

ever, it is assumed that the anilinium ion may be displaced from the BAS by excess 1,3-cyclohexadiene. Less-basic amines form less-stable anilinium ions and are more readily displaced. Assuming equal diffusion rates, the linear correlation reflects the concentration of sites **a** and **b** in the material.

Deviation of 2-methoxyaniline from the above relationship is tentatively explained by the larger minimum kinetic diameter of the N-(cyclohex-2-enyl)-2-methoxyaniline (**6**), which hinders **6** from diffusing out of the pores. In addition, aniline with a methoxy substituent in the *ortho* position may entail greater constraints for the transition state during the nucleophilic attack (partial shielding of the $-NH_2$ group). In the same way, the relatively high rate observed for the parent aniline might be due to the shorter length of products **1** and **2** relative to the corresponding products of the substituted anilines, thus providing for a higher diffusion rate.

4. Conclusion

Zeolite catalysts with 12-membered ring openings, such as H-BEA, can efficiently catalyze the reaction between aniline and 1,3-cyclohexadiene. Generally, the rate is higher for electron-poor (i.e., less-basic) anilines. Thus it seems apparent that the acid-catalysed reaction between 1,3-cyclohexadiene and (the much more basic) aliphatic amines is more difficult to realize. Mechanistically, the key step seems to be the adsorption of 1,3-cyclohexadiene at the BAS and protonation to the

corresponding allyl or enyl cation. More-basic anilines adsorb more strongly at BAS, leading to a lower concentrations of protonated 1,3-cyclohexadiene molecules and, consequently, lower rates of reaction.

Acknowledgments

The authors thank Xaver Hecht and Martin Neukamm for experimental support.

References

[1] T.E. Müller, M. Beller, Chem. Rev. 98 (1998) 675.
[2] P.W. Roesky, T.E. Müller, Angew. Chem. 115 (2003) 2812.
[3] F. Alonso, I.P. Beletskaya, M. Yus, Chem. Rev. 104 (2004) 3079.
[4] J. Seayad, A. Tillack, C.G. Hartung, M. Beller, Adv. Synth. Catal. 344 (2002) 795.
[5] T.E. Müller, in: I.T. Horváth (Ed.), Encyclopedia of Catalysis, Wiley, New York, 2002, p. 492.
[6] R. Taube, in: B. Cornils, W.A. Herrmann (Eds.), Applied Homogeneous Catalysis with Organometallic Compounds, vol. 1, VCH, Weinheim, 1996.
[7] For mechanistic background see, e.g., H.M. Senn, P.E. Blöchl, A. Togni, J. Am. Chem. Soc. 122 (2000) 4098.
[8] J.R. Petersen, J.M. Hoover, W.S. Kassel, A.L. Rheingold, A.R. Johnson, Inorg. Chim. Acta 358 (2005) 687.
[9] L.K. Vo, D.A. Singleton, Org. Lett. 6 (2004) 2469.
[10] B. Kalita, K.M. Nicholas, Tetrahedron. Lett. 46 (2005) 1451.
[11] A. del Zotto, W. Baratta, A. Felluga, P. Rigo, Inorg. Chim. Acta 358 (2005) 2749.
[12] N.T. Patil, N.K. Pahadi, Y. Yamamoto, Tetrahedron. Lett. 46 (2005) 2101.
[13] D.P. Klein, A. Ellern, R.J. Angelici, Organometallics. 23 (2004) 5662.
[14] L.M. Lutete, I. Kadota, Y. Yamamoto, J. Am. Chem. Soc. 126 (2004) 1622.
[15] S. Hong, T.J. Marks, J. Am. Chem. Soc. 124 (2002) 7886.
[16] T. Minami, H. Okamoto, S. Ikeda, R. Tanaka, F. Ozawa, M. Yoshifuji, Angew. Chem. 113 (2001) 4633.
[17] J. Bodis, T.E. Müller, J.A. Lercher, Green Chem. 5 (2003) 227.
[18] O. Löber, M. Kawatsura, J.F. Hartwig, J. Am. Chem. Soc. 123 (2001) 4366.
[19] M. Kawatsura, J.F. Hartwig, J. Am. Chem. Soc. 122 (2000) 9546.
[20] See, e.g., T.E. Müller, J.A. Lercher, V.N. Nguyen, AIChE J. 49 (2003) 214.
[21] M. Utsunomiya, J.F. Hartwig, J. Am. Chem. Soc. 126 (2004) 2702.
[22] K. Tanabe, W.F. Hölderich, Appl. Catal. A 181 (1999) 399.
[23] A. Chauvel, B. Delmon, W.F. Hölderich, Appl. Catal. 115 (1994) 173.
[24] V. Taglieber, W.F. Hölderich, R. Kummer, W.D. Mross, G. Saladin, US 4929758 (1990), to BASF AG.
[25] J. Penzien, T.E. Müller, J.A. Lercher, Microporous Mesoporous Mater. 48 (2001) 285.
[26] J. Penzien, C. Haeßner, A. Jentys, K. Köhler, T.E. Müller, J.A. Lercher, J. Catal. 221 (2004) 302.
[27] V. Neff, T.E. Müller, J.A. Lercher, J. Chem. Soc., Chem. Commun. 8 (2002) 906.
[28] S. Breitenlechner, M. Fleck, T.E. Müller, A. Suppan, J. Mol. Catal. A 214 (2004) 175.
[29] L. Borreto, M.A. Camblor, A. Corma, J. Perez-Pariente, Appl. Catal. 82 (1992) 37.
[30] K.S.N. Reddy, B.S. Rao, V.P. Shiralkar, Appl. Catal. 95 (1993) 53.
[31] C.A. Emeis, J. Catal. 141 (1993) 347.
[32] J. Penzien, A. Abraham, J.A. van Bokhoven, A. Jentys, T.E. Müller, C. Sievers, J.A. Lercher, J. Phys. Chem. B 108 (2004) 4116.
[33] D.M. Roberge, H. Hausmann, W.F. Hölderich, Phys. Chem. Chem. Phys. 4 (2002) 3128.
[34] C. Costa, J.M. Lopes, F. Lemos, F. Ramoa Ribeiro, J. Mol. Catal. A 144 (1999) 221.
[35] J.P. Marques, I. Gener, P. Ayrault, J.C. Bordado, J.M. Lopes, F. Ramoa-Ribeiro, M. Guisnet, Microporous Mesoporous Mater. 60 (2003) 251.
[36] J.B. Higgins, R.B. La Pierre, J.L. Schlenker, A.C. Rohrman, J.D. Wood, G.T. Kerr, W.J. Rohrbaugh, Zeolites 8 (1988) 446.
[37] R.J. Gorte, Catal. Lett. 62 (1999) 1.
[38] J.A. Lercher, G. Ritter, H. Vinek, J. Colloid Interface Sci. 106 (1985) 215.
[39] J. Penzien, T.E. Müller, J.A. Lercher, J. Chem. Soc., Chem. Commun. 18 (2000) 1753.
[40] S. Yang, J.N. Kondo, K. Domen, Catal. Today 73 (2002) 113.
[41] S. Spange, S. Adolph, R. Walther, Y. Zimmermann, J. Phys. Chem. B 107 (2003) 298.
[42] J. Pawlas, Y. Nakao, M. Kawatsura, J.F. Hartwig, J. Am. Chem. Soc. 124 (2002) 3669.